Smart Materials and
Structures

PURPOSE-LED
PUBLISHING™

PAPER

Distinct failure modes in bio-inspired 3D-printed staggered composites under non-aligned loadings

To cite this article: Viacheslav Slesarenko *et al* 2017 *Smart Mater. Struct.* **26** 035053

View the article online for updates and enhancements.

You may also like

- Bibliometric analysis of global research trends on biomimetics, biomimicry, bionics, and bio-inspired concepts in civil engineering using the Scopus database
Naim Sedira, Jorge Pinto, Isabel Bentes et al.
- Dynamic analysis of bio-inspired staggered composites with shear-thickening matrix
Meiqin Yang, Junjie Liu and Qingsheng Yang
- Bio-inspired composites with functionally graded platelets exhibit enhanced stiffness
Sanjay Tapse and S Anup

This content was downloaded from IP address 132.230.196.78 on 04/11/2026 at 15:55

IOP Publishing Smart Materials and Structures
Smart Mater. Struct. 26 (2017) 035053 (8pp) https://doi.org/10.1088/1361-665X/aa59eb

Distinct failure modes in bio-inspired 3D-printed staggered composites under non-aligned loadings

Viacheslav Slesarenko[1,2,3], Nikita Kazarinov[2] and Stephan Rudykh[1]

[1] Technion—Israel Institute of Technology, Haifa, Israel
[2] Lavrentyev Institute of Hydrodynamics of RAS, Novosibirsk, Russia

E-mail: sl.slesarenko@gmail.com

Received 3 August 2016, revised 21 November 2016
Accepted for publication 19 December 2016
Published 21 February 2017



Abstract

The superior mechanical properties of biological materials originate in their complex hierarchical microstructures, combining stiff and soft constituents at different length scales. In this work, we employ a three-dimensional multi-materials printing to fabricate the bio-inspired staggered composites, and study their mechanical properties and failure mechanisms. We observe that bio-inspired staggered composites with inclined stiff tablets are able to undergo two different failure modes, depending on the inclination angle. We find that such artificial structure demonstrates high toughness only under loading applied at relatively small angle to the tablets stacking direction, while for higher angles the composites fail catastrophically. This aspect of the failure behavior was captured experimentally as well as by means of the finite element analysis. We show that even a relatively simple failure model with a strain energy limiter, can be utilized to qualitatively distinguish these two different modes of failure, occurring in the artificial bio-inspired composites.

Keywords: bio-inspired materials, failure, hyperelasticity, non-aligned loading, staggered composites, nacre

(Some figures may appear in colour only in the online journal)

Introduction

Through millions of years of evolution, nature created various biological materials with remarkable mechanical properties despite the significant limitations of the available constituents. For example, teeth of limpets can withstand a tensile stress of 4.9 GPa [1], which makes them one of the strongest known biological materials. The key to the outstanding properties, demonstrated by the natural materials, lays in their complex hierarchical structures, combining stiff and soft components. Depending on the geometry and the properties of constituents, the mechanical properties of natural materials can be varied in the wide range. In the case of bone, for instance, higher mineralization usually makes the bone stiffer, but at the same time more brittle [2, 3]. Materials with superior mechanical properties can be produced—despite the poor set of available constituents—through the use of hierarchical designs [4]. Moreover, a higher level of hierarchy in many cases results in enhanced mechanical properties of materials in terms of stiffness and toughness [5].

Bones and teeth are the examples of so-called 'mineralized tissues' with a staggering arrangement of stiff inclusions, bonded by a softer material [6, 7]. Another example is nacre, which can be found in many seashells. Nacre is a staggered composite made of microscopic mineral tablets with high aspect ratio, arranged in a three-dimensional fashion [8]. Rigid micrometer size tablets usually represent around 95% of the composite volume, while remaining volume is filled by soft interfaces. Mechanical tests on the variety of seashells and nacres [9, 10] revealed the high value of their Young modulus, ranging from 40 to 70 GPa. The mechanical behavior of natural nacre has been studied for different deformation modes, namely uniaxial tension, uniaxial compression and simple shear [11–15]. It has been

[3] Author to whom any correspondence should be addressed.

© 2017 IOP Publishing Ltd Printed in the UK
All rights, including for text and data mining, AI training, and similar technologies, are reserved.

shown that the geometry of nacre is naturally designed to better withstand the loading aligned with the orientation of the elongated tablets, and be able to deform up to relatively high levels of strain without a loss of integrity [16]. Several mechanisms, acting on the different length scales, provide the enhanced mechanical performance of nacre. However, the common observation is that the mechanical properties are mostly defined by the interaction of tablets. For instance, the waviness of the tablets surfaces leads to the actuation of interlocking mechanisms, which increase the resistance of tablet sliding [14]. On the nanoscale level, the peculiarities of the polymeric chains, which are able to unfold during local shear deformation [17], or the formation of aragonite bridges between tablets [18] may affect the overall response of nacre. Therefore, understanding of the peculiarities of the tablets interactions and the mechanical properties of soft bonding interfaces is necessary to explain the enhanced performance of nacres and staggered natural composites in general. In particular, interfaces in such composites should be relatively 'weak' in order to localize deformation in the interfaces and prevent the failure of the stiff tablets [19]. Such weak interfaces with low toughness provide the path for a crack to grow. The aspect ratio of tablets defines the amount of interfaces, available for shearing, therefore staggered composites with higher aspect ratio usually have higher toughness under the loading aligned with the direction of tablets [20]. Interestingly, some imperfections in the nacre microstructure may lead to drastic change of the mechanical properties [21–25]. For example, the brick-and-mortar structures with non-uniform bricks arrangement exhibit poor toughness and fracture resistance as compared to their perfectly arranged counterparts [26].

Since natural composite materials can inherit the beneficial properties of their constituents and conceal their flaws, the bio-inspired material design has attracted significant attention [27]. For example, the nacreous brick-and-mortar microstructures have been mimicked using different techniques by assembling non-organic tablets and polymeric matrix on the different length scales [28–31]. It appears that in general artificial bio-inspired materials reflect the performance of their natural counterparts. Artificial nacreous composites, for instance, demonstrate high stiffness, combined with enhanced toughness [30]. Recent developments in the additive materials fabrication techniques open new opportunities for realization of the material design at various length scales. As opposite to the traditional subtractive manufacturing, additive material manufacturing enables one to precisely control not only the geometry, but also the material composition at different length scales. The additive material fabrication, in particular, three-dimensional multimaterial printing has been already employed to mimic the natural materials and structures. For instance, Lin *et al* designed and 3D-printed the bio-inspired suture interfaces and studied the dependence of their mechanical performance on the geometry [32, 33]. Rudykh and Boyce mimicked the fish scale structure to demonstrate the concept of the flexible armor [34]. Dimas *et al* reproduced biological composite topologies, including bone-like, rotated bone-like and bio-calcite microstructures, and compared their mechanical performance with computational models [35].

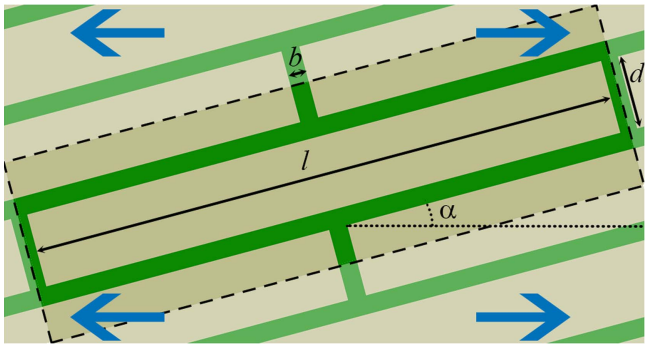


Figure 1. The unit cell of a bio-inspired staggered composite with inclined platelets. The blue arrows represent the direction of the tensile loading.

New manufacturing techniques, such as 3D-printing, provide opportunity to design artificial bio-inspired materials and perform experiments, which are impossible or very challenging on the natural materials. For instance, it is known, that nacreous composites demonstrate best performance under tensile loading along the direction of tablets, while under tensile loading, perpendicular to the direction of tablets, such composite structure fails catastrophically at lower applied force [16]. This anisotropy originates in the microstructure of nacre, and it is essential to understand and predict their mechanical behavior under different deformation modes for possible future applications of such bio-inspired staggered composites. Accurate experiments on the natural seashells are very challenging, however degradation of the performance of nacre under mixed loading modes has been observed [7]. Particularly, the appearance of shear stresses in the interfaces may change the failure mechanisms and decrease the tensile strength in columnar and sheet nacres. In this paper, we address this issue and, through experiments and numerical simulations, we analyze the mechanical behavior of 3D-printed staggered composites with inclined tablets. Moreover, we specifically focus on the failure mechanisms of the bio-inspired composites, subjected to nonaligned loadings. We employ an analytical model with energy limiters, to elucidate the soft interface failure mechanisms observed in our experiments on the 3D printed bio-inspired composites.

Methods and materials

Fabrication and testing

The bio-inspired staggered composite structure has been fabricated with the help of Objet Connex 260 three-dimensional printer. The schematic illustration of the composite periodic structure is shown in figure 1. The geometrical parameters of the staggered composites are $l = 16$ mm, $d = 2$ mm, $b = 0.5$ mm, and the total length, width and thickness of the samples are equal to 130 mm, 40 mm, and 4 mm, respectively. The samples were printed with different inclination angles of the stiff tablets α, varying from 0° to 90°. To study the mechanical properties, the 3D-printed composites were subjected to uniaxial tension using a

universal testing machine Shimadzu EZ-LX. The horizontal displacement of the grips was restricted to maintain the conditions of the macroscopically applied uniaxial tension. The vertical displacement was measured by the displacement of the top grip, and was verified using the point tracking by means of a CCD camera. In order to diminish the rate-dependent behavior of the interface and platelets materials [36, 37], the loading was applied at a low strain rate of $10^{-4}\,s^{-1}$.

Material properties

Through the survey of the mechanical properties of available digital materials, we identified suitable combinations of materials for stiff and soft constituents. In particular, the stiff tablets were printed in VeroWhite polymer (further referred as VW), while the soft interfaces were printed in soft hyperelastic TangoPlus material (further referred as TP). Through the mechanical testing of the homogeneous VW and TP materials, we determined the material constants for both polymers. VW can be described by a linear elastic material model with Young's modulus of $E = 1.8$ GPa and Poisson's ratio $\nu = 0.42$. TP can be considered as a nearly incompressible neo-Hookean material with the shear modulus of $\mu = 0.21$ MPa.

According to our experimental observations, we conclude that the stiff tablets do not break and the staggered composites fail through the failure of the soft interfaces. Different approaches, basing on maximal stress or maximal strain criteria, are widely used to describe and predict the failure of the interfaces, for instance, in the framework of cohesive zone model. In this work, we employ a continuum description of a bulk failure in finite elasticity with energy limiters [38, 39]. These models are basing on the idea of the limited capacity of a material to accumulate the strain energy. The limiter enforces a saturation of the strain energy and indicates the maximum amount of energy that can be stored and dissipated by a material volume element during rupture [38, 40]. For hyperelastic materials, the strain energy depends on the strain through the deformation gradient tensor, thus, this approach is somewhat similar to the maximal strain criteria.

Numerical simulations

The numerical modeling of the staggered composites is performed with the help of finite element code COMSOL 5.1. The models, geometrically identical to the ones used for the 3D-printed sample (see figure 1), are constructed in the finite element model. Since in experiments we induce the shear stresses in soft interfaces via application of the macroscopic tension deformation, in the numerical simulations, we model the whole geometry of the specimen, instead of using a unit cell with periodic boundary conditions. The material of the tablets is modeled as a linear elastic material, with Young modulus and Poisson ratio corresponding to VW polymer. The interfaces are modeled as a neo-Hookean hyperelastic material, which mechanical response is defined by the strain-energy function, integrated in the finite element code as

$$W = \tfrac{1}{2}\mu(I_1(C) - 3) - \mu \ln J + \tfrac{1}{2}\Lambda(\ln J)^2, \qquad (1)$$

where $\boldsymbol{C}$ is the right Cauchy–Green deformation tensor, $J = \sqrt{\det(\boldsymbol{C})}$ and Λ is the first Lame constant. The initial shear modulus μ is chosen to be equal to the shear modulus of TP material. To maintain the nearly incompressible behavior of the soft constituent, we set a high ratio between the shear modulus and the first Lame constant, in particular, $\Lambda = 1000\,\mu$. We separately calculate the strain energy-densities for short (vertical) and long (horizontal) interfaces (see figure 1) and compare these values to analyze the failure behavior in the spirit of the limited strain energy approach.

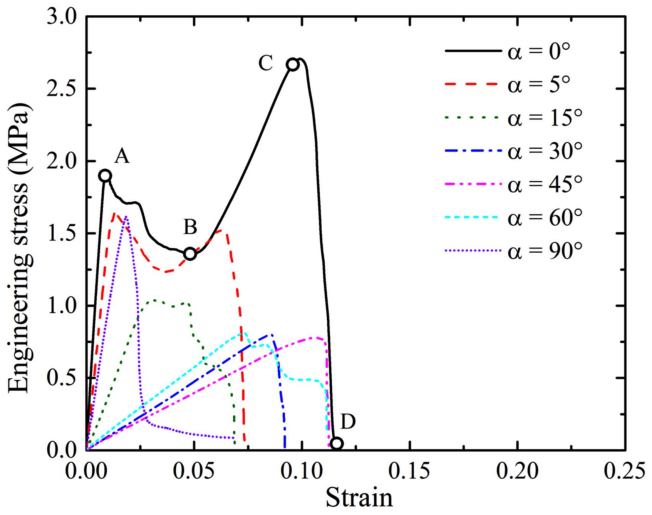


Figure 2. Stress–strain curves, obtained during loading of the staggered composites with inclined tablets. The circles on the black solid curves correspond to the snapshots of the sample, shown in figure 3.

Results and discussion

The 3D printed staggered composites with different inclination angles of tablets are subjected to uniaxial tension. In the aligned composites with inclination angle $\alpha = 0°$, the short interfaces (see figure 1) undergo tensile deformation and long interfaces experience the shear deformation mode. However, in the non-aligned staggered composites with nonzero inclination angles, both modes of deformation are activated. Figure 2 represents the experimentally obtained dependences of the engineering stress, calculated as the applied force divided by cross-section of an undeformed sample, on the strain for the composites with various inclination angles α. The black solid curve corresponds to the mechanical response of the composite with $\alpha = 0°$. One may see that, at the first stage ($\varepsilon < 0.01$), the stiffness of this sample significantly exceeds the stiffness of the specimens with nonzero inclination angles. However, after reaching some critical strain, the sharp drop in the stress is observed. A subsequent loading leads to an increase in the stress level until the complete failure of the sample. We observe a similar behavior for the

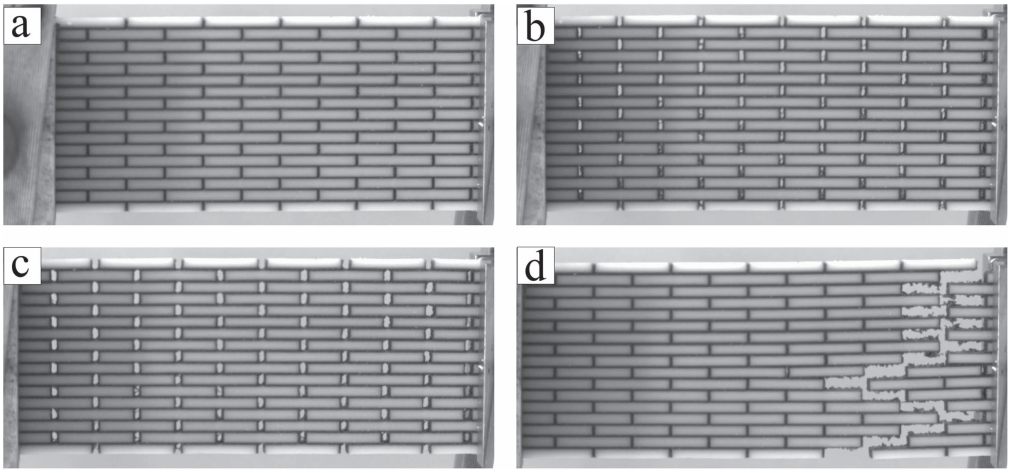


Figure 3. Snapshots of the experiment on nacre with $\alpha = 0°$ at the points A (a), B (b), C (c), D (d) (see figure 2).

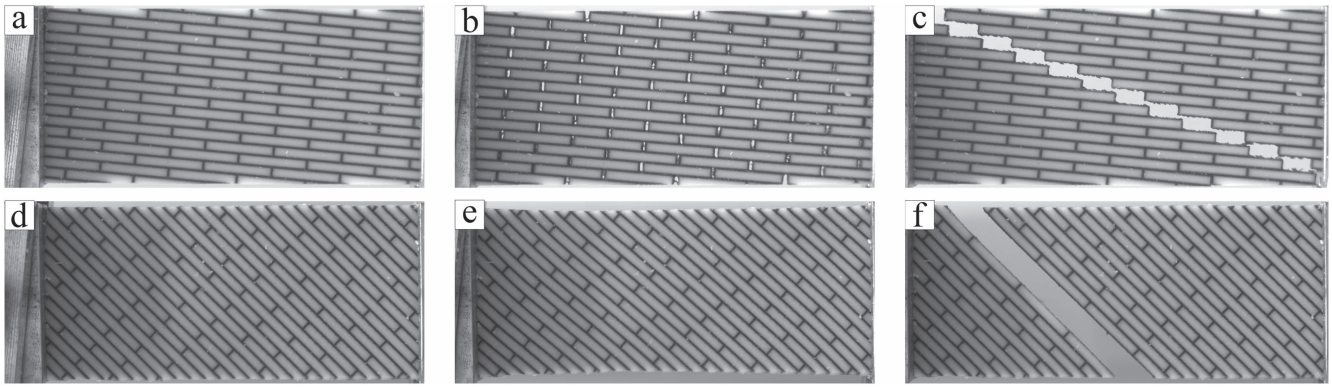


Figure 4. Snapshots of the experiments on staggered composites with $\alpha = 5°$ (a)–(c) and $\alpha = 45°$ (d)–(f), showing the different failure sequences.

samples with $\alpha = 5°$ and $\alpha = 15°$, while the samples with larger inclination angles exhibit a one-stage catastrophic failure after reaching their critical strain. To elucidate the reasons for the distinct failure mechanisms of the samples with different inclination angles, let us first consider figure 3, which shows the snapshots of the aligned composite sample with $\alpha = 0°$. The snapshots are captured at different loading points (A, B, C, D), corresponded to the strain levels of 1%, 5%, 10% and 12%, respectively.

We observe that after reaching some critical strain ($\varepsilon \approx 0.01$, point A at the stress–strain curve), the soft material at the short interfaces fails, leading to a drop in the stress level during following loading. Then the shear deformation in the soft matrix along the long edges of tablets dominates until approximately point C, soon after which the critical level of deformation in the remaining interfaces is reached, and the material loses its integrity. Thus, the specific shape of the stress–strain curve, observed for the specimen with $\alpha = 0°$ is associated with the multi-step failure sequence of the soft interfaces.

Figure 4 shows the experimental snapshots, obtained during the tensile loading of the samples with inclination angles $\alpha = 5°$ (a) and $\alpha = 45°$ (b). We observe a significant difference between the failure mechanisms of these two cases. In particular, the sample with $\alpha = 5°$ exhibit the failure of the short interfaces, which outruns the failure of the long interfaces in a similar manner as for the sample with $\alpha = 0°$ (figure 3). At the same time, for the specimen with $\alpha = 45°$, the failure of the long interfaces occurs earlier, and it leads to a catastrophic loss of integrity after reaching the corresponding critical strain level. There is no such strain, for which the composite retains the load bearing capacity, while some of internal interfaces are broken. Figure 5 shows schematically the failure sequences and the crack paths, experimentally observed in the composites with other inclination angles. Comparing figures 2 and 5, we conclude that the specific shape of the stress–strain curves, observed during the tensile loading of the samples with relatively small inclination angles (0°, 5° and 15°) is caused by the two-step failure of the staggered composite, while the specimens with larger inclination angles (30°, 45°, 60° and 90°) demonstrate almost linear stress–strain dependence until a catastrophic failure. It is worth mentioning, that the sample with $\alpha = 90°$ demonstrates a higher stiffness, which is almost comparable with the stiffness of the sample with $\alpha = 0°$. This is due to the absence of the shearing in the long interfaces, which results in a softer response of the composite material. However, the critical strain, corresponding to the single-step catastrophic failure of the sample for composite with $\alpha = 90°$ is about five times lower in comparison with the composite with $\alpha = 0°$.

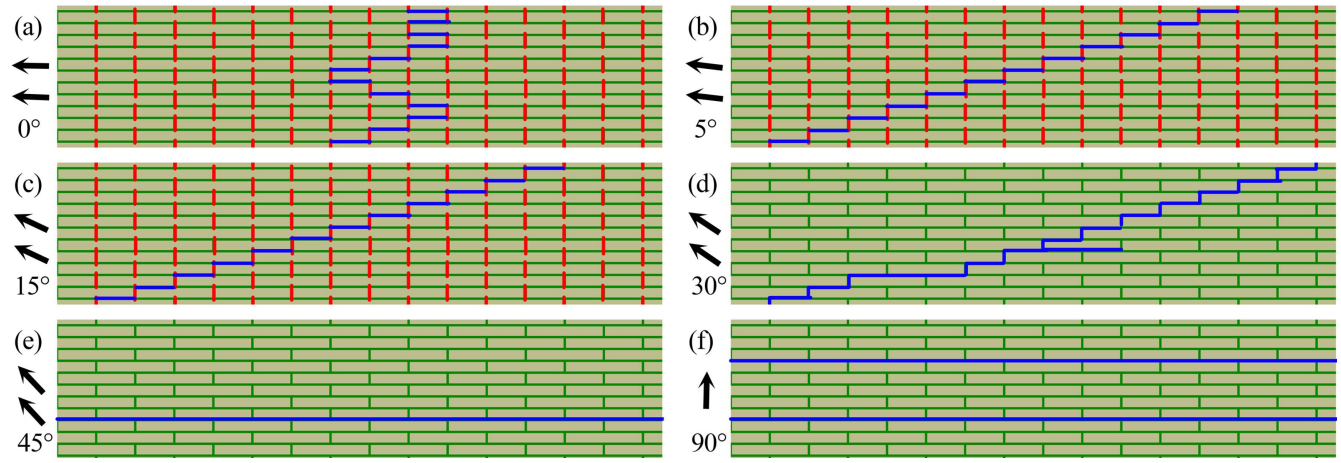


Figure 5. The crack path in staggered composites with different inclination angles. Interfaces colored by red fail first, then the crack propagates along blue path.

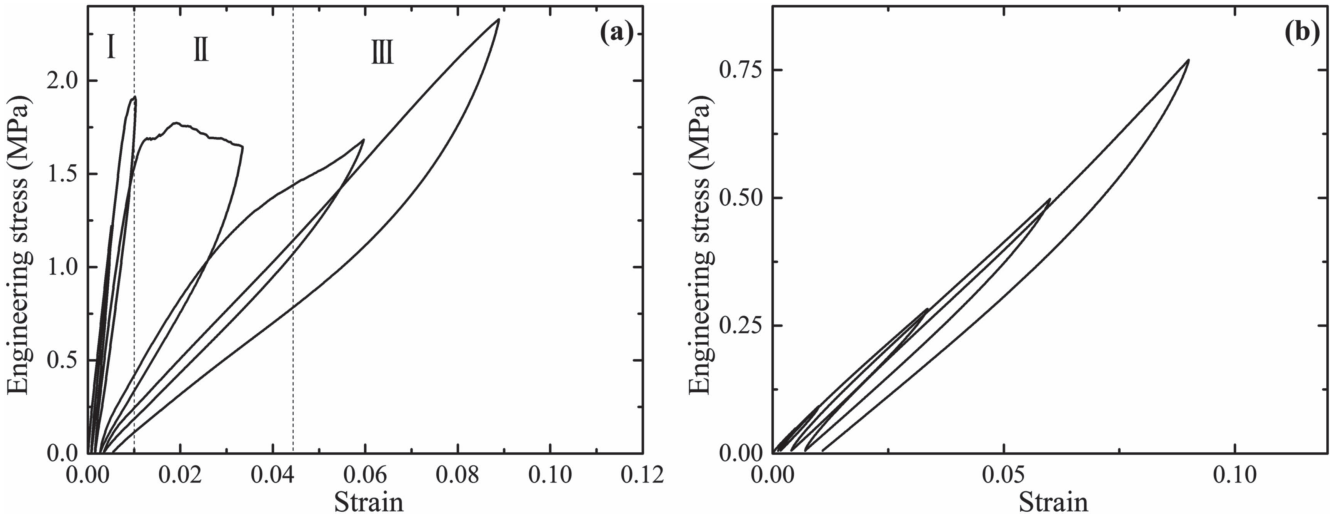


Figure 6. Stress–strain curves experimentally observed during simple tensile loading with sequential loading/unloading cycles for the staggered composites with $\alpha = 0^\circ$ (a) and $\alpha = 45^\circ$ (b). The only complete loading–unloading cycles preceding the failure are shown.

While the sample with $\alpha = 0^\circ$ is able to withstand deformation up to 10% without complete breakage, the sample with $\alpha = 90^\circ$ loses the load bearing capacity at the strain level of about 2%.

In order to investigate the mechanical behavior of the 3D-printed staggered composites after an initial failure of short interfaces, we perform the tensile test of the specimen with $\alpha = 0^\circ$ with sequential loading/unloading cycles. For comparison, we perform the same experiment for the sample with $\alpha = 45^\circ$, which demonstrates only single step failure. Figure 6 shows the experimentally observed stress–strain curves with sequential loading/unloading cycles for the specimens with $\alpha = 0^\circ$ (a) and $\alpha = 45^\circ$ (b). One may see that, for the sample with $\alpha = 45^\circ$, the subsequent loading repeats the unloading path for all reached strain levels. We observe an insignificant accumulation of inelastic strain during load–unload cycles, probably caused by the viscoelastic response of the used materials. However, the amount of the inelastic strain is negligible and the overall mechanical behavior of the composite with $\alpha = 45^\circ$ remains elastic (or hyperelastic) till failure. A similar accumulation of the inelastic strain was experimentally observed by Espinosa *et al* [41]. Contrary to the previous case, the composite with $\alpha = 0^\circ$, loaded along the direction of the stiff tablets, demonstrates a significantly different mechanical behavior. When the strain level does not exceed the strain level, at which the short interfaces break (region I), an increase in strain during the load–unload cycle leads to the subsequent increase in stress. At the same time, after the failure of the short interfaces the following loading cycles do not reach the peak stress, and the maximal stress level at the load–unload cycle drops (region II). When the stress level reaches its minimal value, the following increase in strain leads to an increase in stress, and the load curve in the region III becomes almost linear. Comparing the effective Young modulus of the composite, which can be estimated as the slope of the stress–strain curve on the load–unload cycle, we can conclude that the overall stiffness of the staggered composite with $\alpha = 0^\circ$ drops after the failure of the short interfaces, perpendicular to the direction of loading. We should mention that the similar

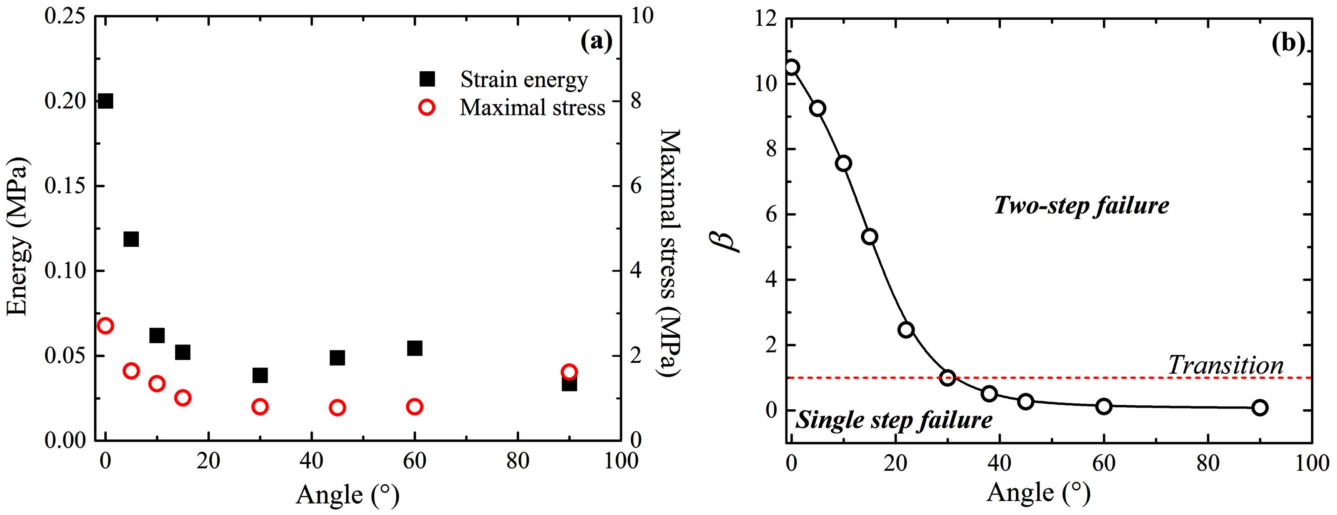


Figure 7. Experimentally obtained dependences of the strain energy (area under the stress–strain curve) and maximal stress on the inclination angle (a). Numerically calculated dependence of the ratio β on the inclination angle. (b) The dashed line represents the transition between the two-step and single step failure modes of the staggered composites.

behavior has been reported by Lin *et al* [33] for the suture interfaces with various geometries. The stress–strain curve, observed for the sutures after the failure of the bounded tip interfaces, matches the stress–strain curve, observed for the sutures without additional tip interfaces. The similar shapes of the stress–strain curves were also found and reported for natural nacreous composites [41] and artificial bone-like structures [42]. Generally speaking, failure of the internal interfaces in the staggered composites leads to the change of internal geometry of the specimen. In other words, the staggered composite, subjected to tensile loading, may be considered as a medium, which undergoes deformation-induced structural changes. The constitutive models, taking into account such structural transformations, were considered, for instance, by Rajagopal and Wineman [43] and De Tommasi *et al* [44, 45]. In the framework of these models, the new deformation micromechanisms can be actuated, when specific activation criteria is met. It leads to a change in the mechanical behavior of the materials and, therefore, to a variation of their stress–strain response. For instance, here we can see that the partial failure of the interfaces leads to the change of the slope of the stress–strain curve (figures 2 and 6(b)). For some strain levels, the slope of the stress–strain curve, is negative, which is partially caused by the reduction of the effective cross-section of the specimen. We should notice, that this deformation mode, when an increase in strain leads to a decrease in stress is unstable and corresponds to the case of localized damage [46].

Thus, we show that the 3D-printed staggered composites with relatively small inclination angles demonstrate two-step failure sequence. First, the failure of short interfaces occurs, followed by a catastrophic loss of integrity of the sample due to the failure of long interfaces. At the same time, the staggered composites with higher inclination angles fail catastrophically after reaching the critical strain level. This drastic difference in the failure mechanisms significantly affects the toughness of the composite. Figure 7(a) shows the toughness of the staggered composites, calculated as the area under the strain–stress curves. Indeed, we observe that the toughness drops, when the failure mechanism changes from the two-step to single step mode.

Next we make use of the hyperelastic model with energy limiter to numerically simulate the change in the failure mechanisms from two-step to a single step mode. Since the critical strain energy-density W_{cr} of the soft phase defines the failure of the material, we calculate the average values of the strain energy-density for short (W^s) and long interfaces (W^l) separately (see figure 1). We introduce the ratio $\beta = W^s/W^l$ between these two components. Figure 7(b) represents the dependence of the ratio β on the inclination angle α, obtained by means of FE simulations.

When the value of $\beta > 1$, the strain energy-density in short interfaces W^s reaches the critical value W_{cr} at a lower strain in comparison with W^l. Thus, for $\beta > 1$ a two-step failure of the nacre-like composite is expected. On the contrary, the case of $\beta > 1$ corresponds to a single step failure mode, observed in composites with high inclination angles. According to figure 7 the transition point, when the failure mode, switches corresponds to the nacre-like composite with inclination angle around 30°. Experimentally, we observe such transition for the composite with inclination angle between 15° and 30°, showing a good agreement with numerical simulations. The slight inconsistency between the experiments and numerical simulations may be caused by applied assumption, regarding the rate-independent behavior of soft material, as well as with averaging of the energy density in the interfaces instead of considering the energy in each material point separately. The transition from the so-called columnar failure mode to the stair failure mode was predicted in nacreous composites by means of the finite element analysis and failure model with maximal stress criteria [7]. While Rabiei *et al* [7] applied shear deformation directly to the unit cell in their numerical simulations, here we use a more practical approach, inducing a mixed strain state in the

interfaces via application of the macroscopic tensile loading non-aligned with the direction of the tablets. Through the experiments we showed that the transition from the columnar failure to the stair failure indeed leads to a drop in the tensile strength, observed in figure 7(a). We determined that for large inclination angles, another mode of deformation may occur, when the interaction between layers is not present, and the staggered composite completely loses its integrity through the failure of only one layer. We conclude by noting, that the failure model for hyperelastic materials, based on the strain energy limiter, adequately predicts the distinct failure mechanisms in bio-inspired staggered composites with inclined tablets. This modeling approach holds a potential for application in more complex composite structures.

Conclusions

We used three-dimensional printing to fabricate bio-inspired staggered composites. Through the experiments and numerical simulations, we investigated their mechanical properties and failure mechanisms. It was shown, that the bio-inspired composites with small inclination angles of the tablets demonstrate relatively high toughness under uniaxial tension. At the same time, staggered composites with high inclination angles fail at relatively low stresses. While in the former case, the composite does not completely lose its load-bearing capacity after partial breakage of the interfaces, for high inclination angles the failure is catastrophic and happens in single step once the critical strain level is achieved. The transition between these two failure modes was observed experimentally, as well as with the help of the finite element simulations. It was shown that relatively simple models of hyperelastic material with energy limiters were able to qualitatively describe the experimentally observed distinct failure mechanisms.

Acknowledgments

VS and NK acknowledge the support provided by the Russian Science Foundation through project 15-11-10000. SR gratefully acknowledges the support of the Israel Science Foundation (grants 1550/15 and 1973/15), and the Taub Foundation through the Horev Fellowship—Leaders in Science and Technology. VS and SR conceived the idea of this paper, VS conducted the experiments, VS and NK performed finite element analysis. All authors took part in the manuscript preparation.

References

[1] Barber A H, Lu D, Pugno N M and Barber A H 2015 Extreme strength observed in limpet teeth *J. R. Soc. Interface* **12** 20141326

[2] Currey J D 1999 The design of mineralised hard tissues for their mechanical functions *J. Exp. Biol.* **202** 3285–94

[3] Currey J D, Zioupos P, Davies P and Casino A 2001 Mechanical properties of nacre and highly mineralized bone *Proc. Biol. Sci.* **268** 107–11

[4] Dimas L S and Buehler M J 2012 Influence of geometry on mechanical properties of bio-inspired silica-based hierarchical materials *Bioinsp. Biomim.* **7** 36024

[5] Sen D and Buehler M J 2011 Structural hierarchies define toughness and defect-tolerance despite simple and mechanically inferior brittle building blocks *Sci. Rep.* **1** 1–9

[6] Khayer Dastjerdi A and Barthelat F 2015 Teleost fish scales amongst the toughest collagenous materials *J. Mech. Behav. Biomed. Mater.* **52** 95–107

[7] Rabiei R, Bekah S and Barthelat F 2010 Failure mode transition in nacre and bone-like materials *Acta Biomater.* **6** 4081–9

[8] Barthelat F 2014 Designing nacre-like materials for simultaneous stiffness, strength and toughness: optimum materials, composition, microstructure and size *J. Mech. Phys. Solids* **73** 22–37

[9] Currey J D 1976 Further studies on the mechanical properties of mollusc shell material *J. Zool.* **180** 445–53

[10] Currey J D and Taylor J D 1974 The mechanical behaviour of some molluscan hard tissues *J. Zool.* **173** 395–406

[11] Menig R, Meyers M H, Meyers M A and Vecchio K S 2000 Quasi-static and dynamic mechanical response of *Haliotis rufescens* (abalone) shells *Acta Mater.* **48** 2383–98

[12] Currey J D 1977 Mechanical properties of mother of pearl in tension *Proc. R. Soc.* B **196** 443–63

[13] Barthelat F, Li C-M, Comi C and Espinosa H D 2006 Mechanical properties of nacre constituents and their impact on mechanical performance *J. Mater. Res.* **21** 1977–86

[14] Barthelat F, Tang H, Zavattieri P D, Li C M and Espinosa H D 2007 On the mechanics of mother-of-pearl: a key feature in the material hierarchical structure *J. Mech. Phys. Solids* **55** 306–37

[15] Barthelat F and Espinosa H D 2007 An experimental investigation of deformation and fracture of nacre-mother of pearl *Exp. Mech.* **47** 311–24

[16] Chen P Y, Lin A Y M, Lin Y S, Seki Y, Stokes A G, Peyras J, Olevsky E A, Meyers M A and McKittrick J 2008 Structure and mechanical properties of selected biological materials *J. Mech. Behav. Biomed. Mater.* **1** 208–26

[17] Smith B L, Schaffer T E, Viani M, Thompson J B, Frederick N A, Kindt J, Belcher A M, Stucky G D, Morse D E and Hansma P K 1999 Molecular mechanistic origin of the toughness of natural adhesives, fibres and composites *Nature* **399** 761–3

[18] Song F and Bai Y 2003 Effects of nanostructures on the fracture strength of the interfaces in nacre *J. Mater. Res.* **18** 1741–4

[19] Khayer Dastjerdi A, Rabiei R and Barthelat F 2013 The weak interfaces within tough natural composites: experiments on three types of nacre *J. Mech. Behav. Biomed. Mater.* **19** 50–60

[20] Ji B and Gao H 2004 Mechanical properties of nanostructure of biological materials *J. Mech. Phys. Solids* **52** 1963–90

[21] Munch E, Launey M E, Alsem D H, Saiz E, Tomsia A P and Ritchie R O 2008 Tough, bio-inspired hybrid materials *Science* **322** 1516–20

[22] Launey M E, Munch E, Alsem D H, Barth H B, Saiz E, Tomsia A P and Ritchie R O 2009 Designing highly toughened hybrid composites through nature-inspired hierarchical complexity *Acta Mater.* **57** 2919–32

[23] Jackson A P, Vincent J F V and Turner R M 1990 Comparison of nacre with other ceramic composites *J. Mater. Sci.* **25** 3173–8

[24] Jackson A P and Vincent J F V 1989 A physical model of nacre *Compos. Sci. Technol.* **36** 255–66

[25] Wang R Z, Suo Z, Evans A G, Yao N and Aksay I A 2001 Deformation mechanisms in nacre *J. Mater. Res.* **16** 2485–93
[26] Pro J W, Lim R K, Petzold L R, Utz M and Begley M R 2015 The impact of stochastic microstructures on the macroscopic fracture properties of brick and mortar composites *Extrem. Mech. Lett.* **5** 1–9
[27] Espinosa H D, Rim J E, Barthelat F and Buehler M J 2009 Merger of structure and material in nacre and bone—perspectives on de novo biomimetic materials *Prog. Mater. Sci.* **54** 1059–100
[28] Bin Y H, Fang H Y, Tan Z H, Wu L H and Yu S H 2010 Biologically inspired, strong, transparent, and functional layered organic–inorganic hybrid films *Angew. Chem., Int. Ed.* **49** 2140–5
[29] Bin Y H, Tan Z H, Fang H Y and Yu S H 2010 Artificial nacre-like bionanocomposite films from the self-assembly of chitosan–montmorillonite hybrid building blocks *Angew. Chem., Int. Ed.* **49** 10127–31
[30] Tang Z, Kotov N A, Magonov S and Ozturk B 2003 Nanostructured artificial nacre *Nat. Mater.* **2** 413–8
[31] Wang J, Cheng Q, Lin L and Jiang L 2014 Synergistic toughening of bioinspired poly(vinyl alcohol)-clay-nanofibrillar cellulose artificial nacre *ACS Nano* **8** 2739–45
[32] Lin E, Li Y, Weaver J C, Ortiz C and Boyce M C 2014 Tunability and enhancement of mechanical behavior with additively manufactured bio-inspired hierarchical suture interfaces *J. Mater. Res.* **29** 1867–75
[33] Lin E, Li Y, Ortiz C and Boyce M C 2014 3D printed, bio-inspired prototypes and analytical models for structured suture interfaces with geometrically-tuned deformation and failure behavior *J. Mech. Phys. Solids* **73** 166–82
[34] Rudykh S and Boyce M C 2014 Analysis of elasmoid fish imbricated layered scale-tissue systems and their bio-inspired analogues at finite strains and bending *IMA J. Appl. Math.* **79** 830–47
[35] Dimas L S, Bratzel G H, Eylon I and Buehler M J 2013 Tough composites inspired by mineralized natural materials: computation, 3D printing, and testing *Adv. Funct. Mater.* **23** 4629–38
[36] Slesarenko V and Rudykh S 2016 Harnessing viscoelasticity and instabilities for tuning wavy patterns in soft layered composites *Soft Matter* **12** 3677–82
[37] Chintapalli R K, Breton S, Dastjerdi A K and Barthelat F 2014 Strain rate hardening: a hidden but critical mechanism for biological composites? *Acta Biomater.* **10** 5064–73
[38] Volokh K Y 2013 Review of the energy limiters approach to modeling failure of rubber *Rubber Chem. Technol.* **86** 470–87
[39] Volokh K Y 2010 On modeling failure of rubber-like materials *Mech. Res. Commun.* **37** 684–9
[40] Trapper P and Volokh K Y 2008 Cracks in rubber *Int. J. Solids Struct.* **45** 6034–44
[41] Espinosa H D, Juster A L, Latourte F J, Loh O Y, Gregoire D and Zavattieri P D 2011 Tablet-level origin of toughening in abalone shells and translation to synthetic composite materials *Nat. Commun.* **2** 173
[42] Mirzaeifar R, Dimas L S, Qin Z and Buehler M J 2015 Defect-Tolerant bioinspired hierarchical composites: simulation and experiment *ACS Biomater. Sci. Eng.* **1** 295–304
[43] Rajagopal K R and Wineman A S 1992 A constitutive equation for nonlinear solids which undergo deformation induced microstructural changes *Int. J. Plast.* **8** 385–95
[44] De Tommasi D, Puglisi G and Saccomandi G 2006 A micromechanics-based model for the Mullins effect *J. Rheol.* **50** 495
[45] De Tommasi D, Marzano S, Puglisi G and Saccomandi G 2010 Localization and stability in damageable amorphous solids *Contin. Mech. Thermodyn.* **22** 47–62
[46] De Tommasi D, Puglisi G and Saccomandi G 2008 Localized versus diffuse damage in amorphous materials *Phys. Rev. Lett.* **100** 085502